Research Article

An efficient variable-step P&O maximum power point tracking technique for grid-connected wind energy conversion system

Hassanien Ramadan[1] · Abdel-Raheem Youssef[1] · Hossam H. H. Mousa[1] · Essam E. M. Mohamed[1]

Received: 27 August 2019 / Accepted: 16 November 2019 / Published online: 22 November 2019

Abstract
This paper proposes an efficient modular sector variable-step perturb and observe (VSPO) maximum power point tracking algorithm. The proposed algorithm enhances the speed tracking and minimizes oscillations level problems associated with traditional P&O methods. The routine of generating the variable step sizes depends on splitting the (P–ω) characteristic curve of wind turbines into modular sectors, in which the perturbation step size for each sector is selected by comparing a suggested ratio with another specified ratio designed according to the required accuracy. By continuously observing the distance between the actual rotor speed and the optimal rotor speed, the VSPO technique applies variable perturbation step sizes according to the current operating sector. Moreover, a wind speed estimation technique is used as a replacement of distributed anemometers for tracking the optimal rotor speed at different wind speeds. The studied system configuration includes three-phase back-to-back converter which is used to connect a 1.5 MW permanent magnet synchronous generator into the utility grid. Furthermore, the model predictive control is used for current control loop in the machine-side converter. To demonstrate the performance of the proposed algorithm, its simulation results are compared with the simulation results of conventional P&O technique under step and random wind variations. In addition, the algorithm performance is studied with real wind data (Hokkaido Island, Japan) using MATLAB/SIMULINK environment. Simulation results show that the VSPO ensures the high tracking speed of maximum power point, while the steady-state oscillation is significantly reduced. The proposed algorithm enhances the system efficiency by 3.5% over the conventional one.

Keywords WECS · PMSG · MPPT · P&O · MPC

Abbreviations

WECS	Wind energy conversion system
VS-WECS	Variable-speed WECS
PMSG	Permanent magnet synchronous generator
MPPT	Maximum power point tracking
P&O	Perturb and observe
CPO	Conventional P&O
LS-PO	Large-step P&O
SS-PO	Small-step P&O
VSPO	Variable-step P&O
MPC	Model predictive control
SCIG	Squirrel cage induction generator
HCS	Hill climb searching
DPC	Direct power controller
IPC	Indirect power controller
IC	Incremental conductance
MSC	Machine-side converter
GSC	Grid-side converter
BTBC	Back-to-back converter

List of symbols

T_{em}	Electromagnetic torque
T	Mechanical torque
P	Number of pair poles

✉ Hossam H. H. Mousa, H.Herzallah@eng.svu.edu.eg; Hassanien Ramadan, H.ramadan@eng.svu.edu.eg; Abdel-Raheem Youssef, A.yousaf@eng.svu.edu.eg; Essam E. M. Mohamed, Essam.mohamed@eng.svu.edu.eg | [1]Department of Electrical Engineering, South Valley University, Qena, Egypt.

SN Applied Sciences (2019) 1:1658 | https://doi.org/10.1007/s42452-019-1716-5

λ_m	Flux linkage
f	Vicious damping coefficient
J	Moment of inertia
ω_m	Turbine rotor angular speed
ω_{ref}	Reference rotor speed
ω_{e}	Electric angular rotor speed
C_{p}	Power coefficient
β	Pitch angle
λ	Tip speed ratio
ρ	Air density (Kg/m^3)
R	Turbine radius (m)
V_{w}	Wind speed (m/s)
$A \approx \pi R^2$	Turbine blades swept area (m^2)
$V_{\text{ds,qs}}$	*d*–*q* stator voltage components
$i_{\text{ds,qs}}$	*d*–*q* stator current components

1 Introduction

Driven by the increasing worldwide demand for energy coupled with growing concerns over greenhouse gas emissions, renewable energy sources are becoming an efficient, clean and sustainable alternative to conventional energy sources [1] by supporting some nanotechnology materials and applications [2, 3]. Among these sources, wind energy is considered the most promising source for providing future energy needs [4]. Therefore, extensive development in wind energy conversion system (WECS) design, control, and implementation is carried out across the world, where it is expected that wind energy will account for 20% of global energy by 2030 [5, 6].

A key component in WECS is the wind turbine (WT) which may be operated at fixed speed or variable speed, resulting in two major configurations of WECS as the fixed-speed and variable-speed WECS. Fixed-speed WECS is characterized by simplicity, more reliable and has a lower cost in comparison with variable-speed WECS. On the other hand, employing a variable-speed WECS will realize maximum power extraction resulting in more efficient system with a reduced load transient at different wind speeds [7, 8]. Electric generators such as squirrel cage induction generator (SCIG), doubly fed induction generator or permanent magnet synchronous generator (PMSG) are coupled with the WT for energy conversion. Commercially, the doubly fed generator is the strongest choice for WECS [9, 10]. However, because of higher power density, efficiency, and reliability, PMSG is increasingly employed in WECS [11, 12]. A power electronic interface is deployed to allow the integration of wind energy into the electric grid. A back-to-back converter, composed of a machine-side converter (MSC) and a grid-side converter (GSC), allows the injection of wind energy to the power grid. With an efficient MSC controller, maximum power extraction at varying wind speeds can be realized. To enhance the performance of WECS, advanced control techniques such as model predictive control (MPC) and fuzzy logic control are implemented. MPC is increasingly applied in power electronics converters control owing to the advancement in digital microcontrollers [13]. Despite the computational burden of MPC, its main advantage is the superiority in handing nonlinearity and multi-variable systems [14]. A two-step MPC for WECS has been proposed in [15]. The cost function of MSC is formulated to achieve MPPT and balance of DC link capacitor voltage. To enhance the voltage ride-through capability of WECS, an MPC scheme that depends on the energy stored by generator inertia is developed in [16].

For efficient operation of WECS, several maximum power point tracking (MPPT) algorithms are developed in the literature [7, 17]. These algorithms can be divided into two major groups: the indirect power controller (IPC) and the direct power controller (DPC). IPC includes algorithms such as tip speed ratio (TSR) [18], optimal torque (OT) [19], and power signal feedback control-based methods [20]. The IPC strategies control the output electrical power of WT by maximizing the mechanical power captured from the wind, whereas the DPC methods directly maximize the output electrical power. TSR strategy is characterized by simplicity and fast response, but its performance highly depends on the accuracy of wind speed estimation or measurement techniques. Therefore, high accuracy anemometer is required for measuring the wind speed which would boost the cost of implementation [21, 22]. The OT algorithm is efficient and simple and no prior knowledge of the wind speed is required. However, optimal torques curves or look-up tables based on experiments are essential for this strategy [21, 23]. The other category of MPPT algorithms is the DPC-based strategies which include various methods such as perturb & observe (P&O)/hill climb search (HCS) [24, 25] and incremental conductance (IC) [26]. Generally, DPC strategies are commonly used in WECS due their simplicity and ease of implement [7]. The underlying principle of P&O algorithm is to regulate the rotor speed and observe the change in the output power to ensure maximum power extraction when wind speed is changed. The rotor speed is perturbed using either a large step or a small step, and the change in the output power is examined until the maximum power point is reached. Traditional P&O algorithms apply a large or small fixed step size perturbation. With a fixed large step size, the settling time of the system is reduced; however, large power oscillation will be experienced around the MPP. On the other hand, a small fixed step will greatly reduce the steady-state oscillation at the cost of slower response. Moreover, traditional P&O methods fail under rapidly changing weather conditions [23, 27].

To alleviate the drawbacks of traditional P&O algorithms and to enhance their tracking efficiency, researchers have proposed several adaptive step-size algorithms [8, 28–31]. A modified P&O algorithm that uses two modes of operation, namely normal P&O mode, and predictive mode is proposed in [28]. Under a slow wind speed variation, the normal P&O mode is activated, while in case of rapidly changing wind speed both modes are applied. Authors in [29] have developed an adaptive sensor-less P&O algorithm that handles the loss-tracking and the tracking speed efficiency trade-off problem using the optimal power curve. A two control-stage-based modified MPPT has been proposed in [30]. The algorithm is characterized by high tracking speed and efficiency. However, the knowledge of system parameters is needed for intermediate variables calculation. In Ref [31], an adaptive variable-step P&O algorithm is implemented that uses a PID controller optimized by genetic algorithm (GA) to set the perturbation step size. However, the application of GA increases the complexity of the algorithm. In [32], MPPT controller based on combined power signal feedback and hill climb search algorithm has been developed. This algorithm uses the k_{opt} parameter to set the step size which is determined based on the voltage and current of the DC link. To overcome the slow speed of convergence of conventional P&O, a modified P&O strategy that uses a large forward step and a small reverse step is proposed in [33]. Despite the enhancement in the tracking speed, high oscillations are experienced around the MPP due to the application of large forward fixed step. Moreover, anemometers are deployed to measure the wind speed which increases the cost of implementation. Based on the distance between the operating point and MPP, the step size of a variable-step P&O technique using k_{opt} parameter is developed in [34, 35]. Although the algorithm provides a fast-tracking speed, the need for wind speed measurement and the variation of k_{opt} for different wind speeds are considered the main drawbacks of the algorithm. Moreover, several efficient P&O algorithms are recently proposed in [25, 36–43] to enhance the operation of variable-step-size P&O algorithms.

This paper introduces a fast and efficient VSPO-based MPPT algorithm to overcome the shortcomings of conventional P&O MPPT techniques such as oscillations around the peak power point and speed convergence. The proposed algorithm applies a perturbation step size according to the operating sectors which are defined by comparing two specified ratios. It observes the distance between the optimal rotor speed and the actual rotor speed and perturbs the rotor speed to track the optimal value in which the MPP is located. This algorithm employs the wind speed estimation to calculate the optimal rotor speed at each wind speed. It offers a balance for the trade-off between the rapid speed tracking and the low oscillation levels compared to other P&O algorithms. A WECS consisting of a 1.5 MW PMSG connected to the grid via a BTBC is employed to test the developed algorithm. Furthermore, the MPC is used for the current control loop in the MSC. The performance of the proposed control schemes is validated by real wind data (Hokkaido Island, Japan) using MATLAB/SIMULINK environment. This paper is organized as follows: Sect. 2 provides the mathematical modeling of WT and PMSG. In Sect. 3 and Sect. 4, MSC and GSC control schemes are presented, respectively. The wind speed estimation algorithm is presented in Sect. 5. Section 6 explains the conventional P&O and the proposed variable-step P&O. Calculation of the WECS efficiency is provided in Sect. 7. In Sect. 8, the simulation results are presented and discussed. Finally, conclusions are drawn in Sect. 9.

2 System description

The system scheme of the three-phase WECS studied in this paper is depicted in Fig. 1. The implemented WECS consists of a 1.5 MW three-phase PMSG directly coupled to a wind turbine. The captured wind power is injected into the grid using a fully controlled BTBC interface with a common DC link. BTBC consists of an MSC used to realize the extraction of maximum power from the wind turbine. Moreover, a GSC is implemented to control the DC link voltage and ensures unity power factor operation [7, 44].

2.1 Wind turbine model

In WECS, the wind kinetic power is converted to mechanical power using WT. Input wind power P_w to the WT can be expressed as [45–47]:

$$P_w = \frac{1}{2}\rho\pi R^2 V_w^3 \quad (1)$$

where ρ is the air density (kg/m^3), R is the turbine radius (m), and V_W is the wind speed (m/s). The extracted mechanical power from the wind depends on the power coefficient C_p of the turbine, usually provided by the WT manufacturer. The output mechanical power is given by

$$P_m = \frac{1}{2}\rho\pi R^2 C_p(\lambda,\beta)V_w^3 \quad (2)$$

where $C_P(\lambda,\beta)$ is the power coefficient function, λ is the tip speed ratio, β is the blade pitch angle. For a fixed bitch angle $\beta = 0$, the power coefficient and tip speed ratio are expressed as:

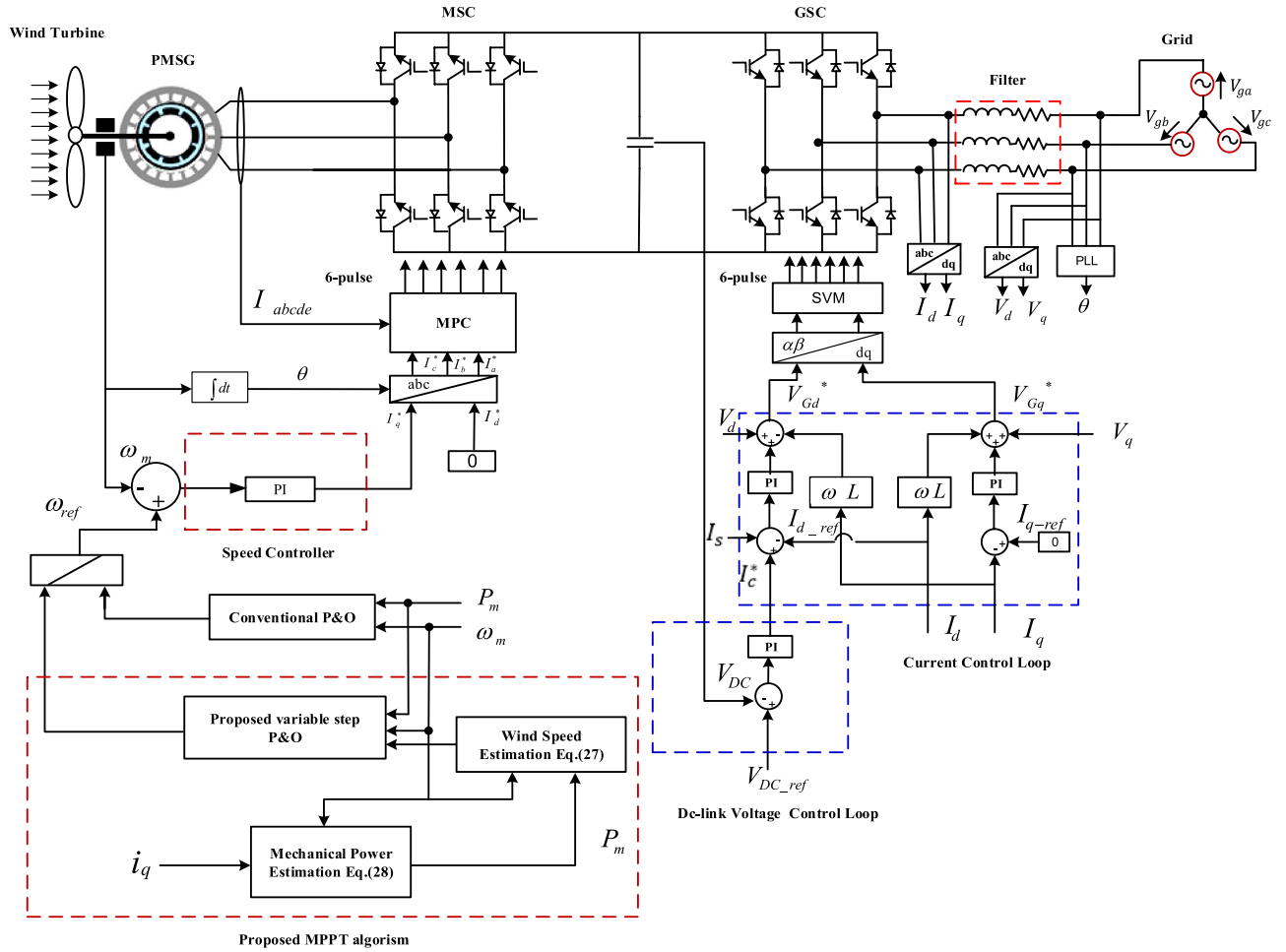

Fig. 1 WECS configuration

$$C_p(\lambda,\beta) = C_1\left(\frac{C_2}{\lambda_i} - C_3\beta - C_4\right)e^{\frac{-C_5}{\lambda_i}} + C_6\lambda \tag{3}$$

$$\lambda_i^{-1} = (\lambda + 0.08\beta)^{-1} - 0.035\left(1+\beta^3\right)^{-1} \tag{4}$$

$$\lambda = \frac{\omega_m R}{V_w} \tag{5}$$

where the approximated coefficient values $c_1 - c_6$ are given in "Appendix 1", Table 3.

From Eq. (2), the output power of WT is maximum when the power coefficient is adjusted at the maximum value $C_{p,}$max. For wind speeds equal to or below the rated value, the WT pitch angle control is deactivated and the pitch angle β is fixed. Hence, according to Eq. (3), the power coefficient C_p can be controlled by varying the tip speed ratio. The variation of the power coefficient with the TSR is depicted in Fig. 3. It can be observed that for maximizing the power coefficient, there is an optimum value of the tip speed ratio at which the extracted mechanical power is maximum. At a particular wind speed, Eq. (5) reveals that the optimum tip speed ratio λ_{opt} can be obtained only by varying the rotor speed. With the instantaneous change of wind speed, the rotor speed must be controlled to ensure the operation at the MPP. Therefore, intelligent controllers must be implemented to regulate rotor speed to attain maximum power with the variation of wind speed. The power–speed (P–ω) characteristic curve of the wind turbine at different wind speeds is shown in Fig. 2 [48]. To obtain maximum power, the value $\frac{dP_m}{d\omega}$ must equal to zero. Applying this condition to Eq. (2) yields

$$\frac{dP_m}{d\omega} = 0.5\rho\pi R^2 V_w^3 \frac{dC_p(\lambda,\beta)}{d\omega} \tag{6}$$

When the pitch angle β is fixed, the power coefficient is a function only of TSR and the value of $\frac{dC_p}{d\omega}$ becomes

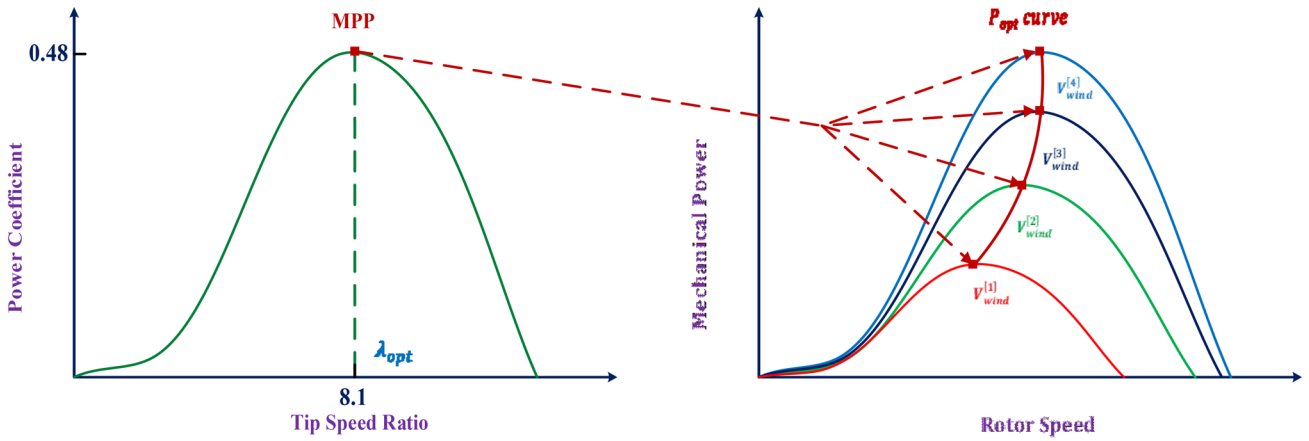

Fig. 2 Power characteristics of WT

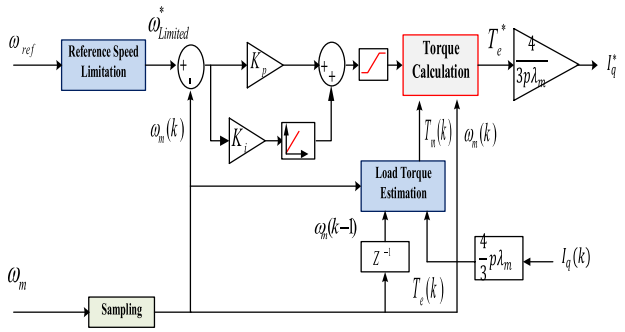

Fig. 3 Speed control details

$$\frac{dC_p}{d\omega} = \frac{dC_p}{d\lambda_i} * \frac{d\lambda_i}{d\omega} \tag{7}$$

Then,

$$\frac{dP_m}{d\omega} = 0.5\rho\pi R^2 V^3 \left(\frac{1260}{\lambda_i^3} - \frac{114.39}{\lambda_i^2}\right) e^{\frac{-21}{\lambda_i}} * \frac{V_w * R}{\left(V_w - 0.035R\omega\right)^2} \tag{8}$$

From Eq. (8), for maximum power extraction the values of λ_{opt} and C_{p-max} are 8.1 and 0.48, respectively.

2.2 The PMSG model

PMSGs are increasingly used in WECSs due to their higher power density, reasonable price, and the ability of coupling to the WT without the need for gearbox at low variation of turbine speed. The *d*-axis and *q*-axis voltages (V_{ds} and V_{qs}) of a surface-mounted PMSG in the *dq* reference frame are described as follows [49]:

$$V_{ds} = R_s i_{ds} + L_d \frac{di_{ds}}{dt} - \omega_s L_q i_{qs} \tag{9}$$

$$V_{qs} = R_s i_{qs} + L_q \frac{di_{qs}}{dt} + \omega_s L_d i_{ds} + \omega_s \lambda_m \tag{10}$$

where i_{ds} and i_{qs} are the direct and quadrature axes stator current, R_s is the stator resistance in ohms, L_d and L_q are the inductances in the d–q-axis, λ_m is the rotor flux linkage in weber, and ω_s is the electrical speed. The torque of the PMSM can be formulated by the following equation

$$T = T_{em} + T_r = \frac{3}{2} \cdot \frac{P}{2} \cdot i_{qs}\left[\lambda_m + \left(L_d - L_q\right) \cdot i_{ds}\right] \tag{11}$$

where T_r and T_{em} are the reluctance and electromagnetic torque, respectively, and P is the poles number.

For surface-mounted PMSG $L_d = L_q$. Consequently, $T_r = 0$ and the machine torque is expressed as:

$$T = T_{em} = \frac{3}{2} \cdot \frac{P}{2} \cdot i_{qs}\lambda_m \tag{12}$$

3 Control of the machine-side converter

For efficient operation of WECS, the WT should operate at MPP. The objective of MSC is to achieve maximum output power from the WT. Therefore, intelligent control is applied to the MSC to ensure the operation at the MPP. The output power of WT is a function of power coefficient C_p Moreover, the C_p depends on tip speed ratio λ, which varies with the rotor speed. To achieve optimal λ that gives maximum power coefficient, the MSC is controlled so that rotor speed tracks a calculated reference speed. The control system of MSC is composed of two control

loops. A speed controller implemented by the outer loop and current control (inner loop) is provided using model predictive control (MPC). The speed controller based on the error between actual and optimal rotor speeds generates a reference value for the q-axis current as depicted in Fig. 3. Referring to Eqs. (13), (14), and solving for $(\mathrm{d}i/\mathrm{d}t)$, expressions for MPC can be obtained as follows:

$$\frac{\mathrm{d}i_{\mathrm{ds}}}{\mathrm{d}t} = -\frac{R_s}{L_d}i_{\mathrm{ds}} + \frac{L_q}{L_d}\omega_s i_{\mathrm{qs}} + \frac{1}{L_d}v_{\mathrm{ds}} \tag{13}$$

$$\frac{\mathrm{d}i_{\mathrm{qs}}}{\mathrm{d}t} = -\frac{R_s}{L_q}i_{\mathrm{qs}} - \frac{L_d}{L_q}\omega_s i_{\mathrm{ds}} - \frac{\Psi}{L_q}\omega_s + \frac{1}{L_q}v_{\mathrm{qs}} \tag{14}$$

Using a sampler of T_s sampling time, Eqs. (13) and (14) are discretized and using Euler approximation a model in the discrete time is obtained. Replacing $(\mathrm{d}i/\mathrm{d}t)$ by the forward Euler approximation yields

$$\frac{\mathrm{d}i}{\mathrm{d}t} = \frac{i(k+1) - i(k)}{T_s} \tag{15}$$

Hence, the PMSG is modeled as:

$$i_d(k+1) = \left(1 - \frac{T_s R_s}{L_d}\right) * i_d(k) + \frac{T_s L_q}{L_d}\omega_e * i_q(k) + \frac{T_s}{L_d}v_d(k) \tag{16}$$

$$i_q(k+1) = \left(1 - \frac{T_s R_s}{L_q}\right) * i_q(k) - \frac{T_s L_d}{L_q}\omega_e * i_d(k) + \frac{T_s}{L_q}v_q(k) - \frac{T_s \Psi}{L_q}\omega_e \tag{17}$$

The MPC cost function, F, is described by:

$$F = \left|i_{\mathrm{dref}}(k+1) - i_d(k+1)\right| + \left|i_{\mathrm{qref}}(k+1) - i_q(k+1)\right| \tag{18}$$

where i_{dref} and i_{qref} are the stator currents reference values in the *d–q* axes.

Seven distinct values corresponding to the seven possible output vectors described in [50] are used to provide a current prediction. The cost function in Eq. (18) is minimized to estimate the converter output vector that should be applied for the next sampling instant.

4 Grid-tie inverter

The connection of the WECS to the utility grid is realized using a grid-tie inverter (GTI). Moreover, the GTI allows the adjustment of the system output voltage with varying atmospheric conditions using the DC link voltage regulation control loop. The GTI controller performs two main tasks: regulating the voltage of the DC link capacitor to its set point which is realized using PI outer control loop. The other task is to regulate both the direct and quadrature currents (I_d and I_q) using an inner PI-based control loop. To operate the GTI at unity power factor, the quadrature current reference $I_{q\text{-ref}}$ is set to zero, as illustrated in Fig. 2.

The phase voltages of the grid as a function of converter voltages and currents are formulated in Eq. (19):

$$\begin{bmatrix} V_{ia} \\ V_{ib} \\ V_{ic} \end{bmatrix} = \begin{bmatrix} R_f \end{bmatrix} \begin{bmatrix} i_{fa} \\ i_{fb} \\ i_{fc} \end{bmatrix} + \begin{bmatrix} \dot{\lambda}_a \\ \dot{\lambda}_b \\ \dot{\lambda}_c \end{bmatrix} + \begin{bmatrix} V_{ga} \\ V_{gb} \\ V_{gc} \end{bmatrix} \tag{19}$$

where R_f and L_f are diagonal matrices, $\dot{\lambda}_a = L_f \frac{\mathrm{d}i_{fa}}{\mathrm{d}t}, \dot{\lambda}_b = L_f \frac{\mathrm{d}i_{fb}}{\mathrm{d}t}$ and $\dot{\lambda}_c = L_f \frac{\mathrm{d}i_{fc}}{\mathrm{d}t}$. The direct and quadrature voltages of the GTI are formulated in Eq. (20).

$$\begin{bmatrix} V_{id} \\ V_{iq} \end{bmatrix} = \begin{bmatrix} r_f \end{bmatrix} \begin{bmatrix} i_{fd} \\ i_{fq} \end{bmatrix} + \begin{bmatrix} \dot{\lambda}_{fd} - \omega_g \psi_{fq} \\ \dot{\lambda}_{fq} + \omega_g \psi_{fd} \end{bmatrix} + \begin{bmatrix} V_{gd} \\ V_{gq} \end{bmatrix} \tag{20}$$

where $\omega_g = 2\pi f_g$, $\psi_{fq} = l_f i_{fq}$, $\psi_{fd} = l_f i_{fd}$, $\dot{\lambda}_{fd} = l_f \frac{\mathrm{d}}{\mathrm{d}t} i_{fd}$, $\dot{\lambda}_{fq} = l_f \frac{\mathrm{d}}{\mathrm{d}t} i_{fq}$. By setting $V_{gq} = 0$, the GTI exchanges no reactive power with the utility grid; hence, unity power factor operation is realized. The voltage of the DC link capacitor is regulated by deploying an outer PI control loop which provides the reference value of the capacitor current expressed in Eq. (21).

$$I_c = \frac{P_e - P_g}{V_{\mathrm{dc}}} = C\frac{\mathrm{d}V_{\mathrm{dc}}}{\mathrm{d}t} \tag{21}$$

where P_e is the MSC active power and P_g is the GTI power. C and V_{dc} are the capacitance and voltage of the DC link capacitor, respectively.Then,

$$i_{fd}^* = I_s - I_c^* \text{ and } I_s = \frac{P_e}{V_{\mathrm{dc}}} \tag{22}$$

where i_{fd}^* is the capacitor reference current in the d-axis. Finally, instantaneous power components injected into the utility grid are expressed as follows:

$$P_g = \frac{3}{2}V_{gd}i_{fd} \tag{23}$$

$$Q_g = \frac{3}{2}V_{gd}i_{fq} \tag{24}$$

5 Wind speed estimation algorithm

The developed algorithm requires knowledge of wind speed. Therefore, accurate anemometer should be used for wind speed measurement. However, the use of anemometer boosts system implementation and maintenance cost and reduces system reliability. To overcome the aforementioned issues with the use of anemometers, wind speed

Table 1 Proposed algorithm parameters

Sector	R_k	
Sector (A)	0.6	$\Delta\omega_1 = 0.2$
Sector (B)	0.4	$\Delta\omega_2 = 0.1$
Sector (C)	0.12	$\Delta\omega_3 = 0.05$
Sector (D)	$0 < \varepsilon < 0.12$	$\Delta\omega_4 = 0.01$

estimation (WSE) techniques are proposed to calculate wind speed without the need for speed sensors. Power coefficient can be formulated as a polynomial equation as follows [51, 52]:

$$C_p = a_0 + a_1\lambda + a_2\lambda^2 + a_3\lambda^3 \tag{25}$$

Equation (25) constants are provided in Table 1. Substituting the value of C_p and λ in Eq. (2), the WT power is given in Eq. (26) as follows:

$$P_{\mathrm{m}} = \frac{\rho\pi R^2 V_{\mathrm{w}}^3}{2}\left(a_0 + a_1\frac{\omega_m R}{V_{\mathrm{w}}} + a_2\left(\frac{\omega_m R}{V_{\mathrm{w}}}\right)^2 + a_3\left(\frac{\omega_m R}{V_{\mathrm{w}}}\right)^3\right) \tag{26}$$

V_{w} is estimated as a function of $P_{\mathrm{m}}, \omega_{\mathrm{m}}$. Simplifying Eq. (26), a polynomial equation for the wind speed which can be solved using numerical methods is derived as follows:

$$V_{\mathrm{w}}^3 + \frac{a_1}{a_0}R\omega_{\mathrm{m}}V_{\mathrm{w}}^2 + \frac{a_2}{a_0}\left(R\omega_{\mathrm{m}}\right)^2 V_{\mathrm{w}} + \frac{a_3}{a_0}\left(R\omega_{\mathrm{m}}\right)^3 - \frac{P_{\mathrm{m}}}{0.5\rho\pi R^2} = 0 \tag{27}$$

The output torque or power can be calculated according to the following equation:

$$P_{\mathrm{m}} = T_m\omega_m = \omega_m\left(J\frac{\mathrm{d}\omega_m}{\mathrm{d}t} + f\omega_m + \frac{3}{2}\cdot\frac{P}{2}\cdot i_{\mathrm{qs}}\lambda_m\right) \tag{28}$$

6 MPPT control

6.1 Conventional P&O MPPT algorithm

To operate at the MPP, the conventional P&O MPPT algorithm varies the generated power according to rotor speed variations until the *P*–*ω* curve slope is zero. The CPO algorithm is not requiring prior WT knowledge and installed anemometer for measuring wind speed. The CPO algorithm perturbs the control variables with specific step size and observes the objective function variation until obtaining the MPP local. This strategy depends on the location of operating point if it is on the left side of the MPP $\Delta P_\omega > 0$; the CPO algorithm varies the generator speed with an increment value to the right near the MPP. Else if the operating point is on the right side $\Delta P_\omega < 0$, the CPO algorithm inverses the perturbing direction as depicted in Fig. 4a. Selecting the step size is considered as the main drawback in this technique. The perturb step size is directly related to the WT performance, such as the settling time and oscillation level of the extracted power. If a large step size is applied, the settling time will be enhanced. However, the oscillation level around the MPP is increased which has a worse effect on the large-scale machines. In contrast, the application of a small step size will result in decreased steady-state oscillations. However, it reduces the speed convergence and increases power loss. To eradicate these drawbacks, modified P&O techniques are utilized which combine features of both types. The CPO MPPT algorithm performance under fixed step size, small or large step sizes, is presented in Fig. 4b, c, respectively.

6.2 Proposed P&O MPPT technique

To get rid of the operating problems of conventional P&O techniques, the proposed P&O algorithm creates a proper equilibrium between MPP tracking and the optimal rotor speed. The proposed algorithm specifies the MPP location by determining the optimal rotor speed. The selection of step sizes and the perturbation direction depends on the distance between the current rotational

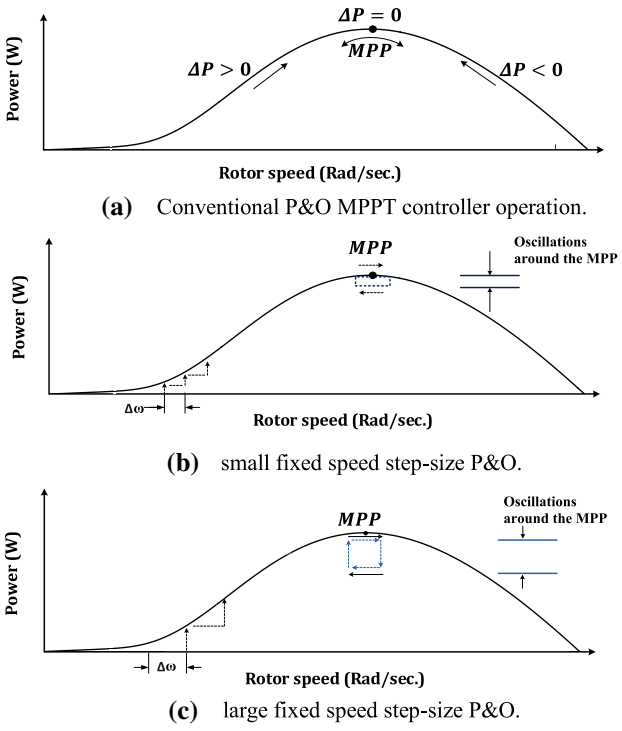

Fig. 4 Conventional P&O MPPT algorithm

speed and the optimal rotational speed during varying optimum curves. This strategy aims to work at the optimal rotor speed in which the MPP is situated. Therefore, this strategy is fast and efficient for MPP tracking that depends on observing only the rotor speed perturbation. It divides the P–ω curve into several operating sectors by applying a proposing ratio ($\left|\frac{\Delta\omega_c}{\omega_{opt}}\right|$) that is associated with a definite ratio (R_k). The k denotes the total number of sectors in forward perturbing direction as well as reverse perturbing direction. R is a ratio where $\varepsilon < R < 1$. ε is the necessary power precision alterations around the MPP. The operation of the proposed P&O algorithm concept is portrayed in Fig. 5. The operation of the proposed algorithm is described as follows. By using the optimal values of the power coefficient and tip speed ratio, the optimal rotor speed is formulated as

$$\omega_{opt} = 8.1\frac{V_{wind}}{R} \tag{29}$$

so the optimal mechanical power at the MPP is

$$P_c = 1.5 \times 10^{-3}\rho R^5\omega_{opt}^3 = K_{opt}\omega_{opt}^3 \tag{30}$$

and the actual power from Eq. (30) becomes

$$P_m = K_{opt}\omega_m^3 \tag{31}$$

From previous equations, the rotor speed is a well-defined objective variable for detecting the MPP by working at the optimal rotor speed condition. The rotor speed is continually perturbed until reaching the MPP.

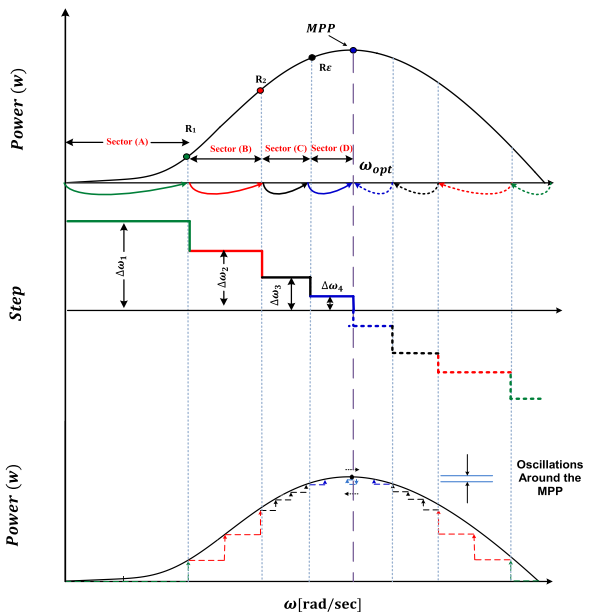

Fig. 5 Variable-step P&O MPPT algorithm operation

To find the optimal rotor speed at wind speed fluctuations, Eq. (29) can be formulated as

$$\omega_{opt2} = \omega_{opt1}\left(\frac{V_{wind2}}{V_{wind1}}\right) \tag{32}$$

By referring previous equation to rated wind speed, optimal rotor speed can be found with respect to the rated wind speed as follows:

$$\omega_{optc} = \omega_{optm}\left(\frac{V_c}{V_m}\right) \tag{33}$$

where ω_{optc} is the optimal rotor speed at the current wind speed (V_c). ω_{optm} and V_m are the optimum rated rotor speed and the rated wind speed, respectively.

Now, the proposed ratio is designed as follows; the optimal rotor speed is calculated from Eq. (34), and knowing the actual rotor speed, the special synthesized ratio is designed as

$$\left|\frac{\Delta\omega_c}{\omega_{optc}}\right| = \left|\frac{\omega_{optc} - \omega_m}{\omega_{optc}}\right| \tag{34}$$

To specify the ratio of each operating sector, the rotor speed at the MPP is compared to the sector border. While the rotor speed is located remote from the MPP, a large step size is considered and continuously decreased closer to the MPP. The proposed P&O algorithm scheme is outlined as:

- Measure $P_\omega(n)$ and $\omega_m(n)$; also estimate the wind speed.
- Calculate $\Delta P_\omega(n)$, ω_{optc}. and $\left|\frac{\Delta\omega_c}{\omega_{optc}}\right|$.
- Select the operating region direction.
- Compare $\left|\frac{\Delta\omega_c}{\omega_{optc}}\right|$ with R_k.
- Disturb the rotor speed with the stated step size of the operating sector.
- Change variables of the proposed P&O algorithm controller.

To validate the proposed algorithm, sector number k equals four in each perturbation direction with several step sizes as demonstrated in Table 1. The step size choice and the number of operating sectors depend on the required power accuracy, settling time and oscillation level around the MPP. The complete proposed algorithm flowchart is described in Fig. 6.

7 WECS efficiency

The overall efficiency of the WECS is used as a performance index to compare the developed algorithm with the conventional P&O technique. The efficiency is

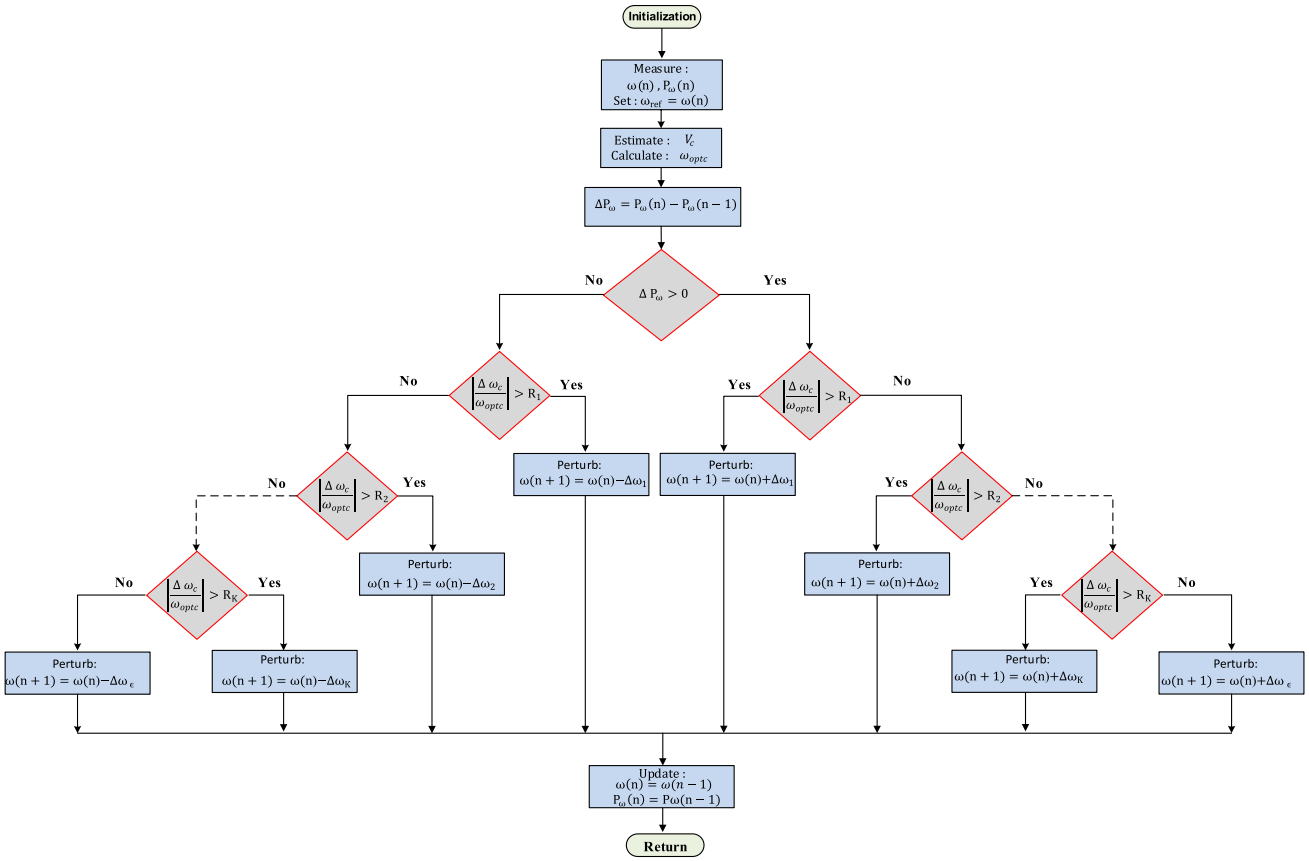

Fig. 6 Flowchart of variable-step P&O MPPT algorithm

estimated as the ratio of the actual output power of the WECS to the theoretical power [53]. This is formulated as

$$\eta_{\text{sys}} = \frac{\int_0^t P_g}{\int_0^t P_{\text{th}}} \cdot 100[\%] \tag{35}$$

where P_{th} and P_g are the theoretical and actual power of the WECS, respectively, and η_{sys} is the overall efficiency of the system.

8 Simulation results and discussion

To validate the effectiveness of the developed MPPT algorithm, simulation results of grid-connected WECS with application of the proposed algorithm P&O are assessed and compared. Different wind speed profiles are employed step change, random, and real wind speed profiles. Parameters of the overall WECS are given in "Appendix 1", Table 3. PI controllers gains of both the MSC and GSC are provided in "Appendix 2", Table 4 as designed in [54].

8.1 Step wind speed

Figure 7 depicts the MSC performance of the proposed and conventional P&O algorithms under a step wind speed change. The wind speed estimation is used to acquire the operating wind speed from the given profile in Fig. 7a. Figure 7b shows that the power coefficient sustains its optimum value, $C_p = 0.48$, which gives an indication that the maximum mechanical power is extracted as portrayed in Fig. 7c. Large step size PO (LS-PO) and small step PO (SS-PO) of conventional P&O algorithm are applied and compared to the proposed P&O algorithm. From Fig. 7b, the speed tracking of LS-PO is faster than both, the SS-PO and the variable-step PO (VSPO), with a settling time of (80 ms). But oscillation levels are large, peak-to-peak rotor speed oscillations = 4 rad/s. The SS-PO has small oscillation level at steady-state condition. On the other hand, speed tracking is slow with settling time (1000 ms.). In contrast, the VSPO has rapid response with and lower settling time of 80 ms and low peak-to-peak oscillation level of 2 rad/s. It is obvious that the C_p average value of the VSPO algorithm is maximum in comparison with both SS-PO and

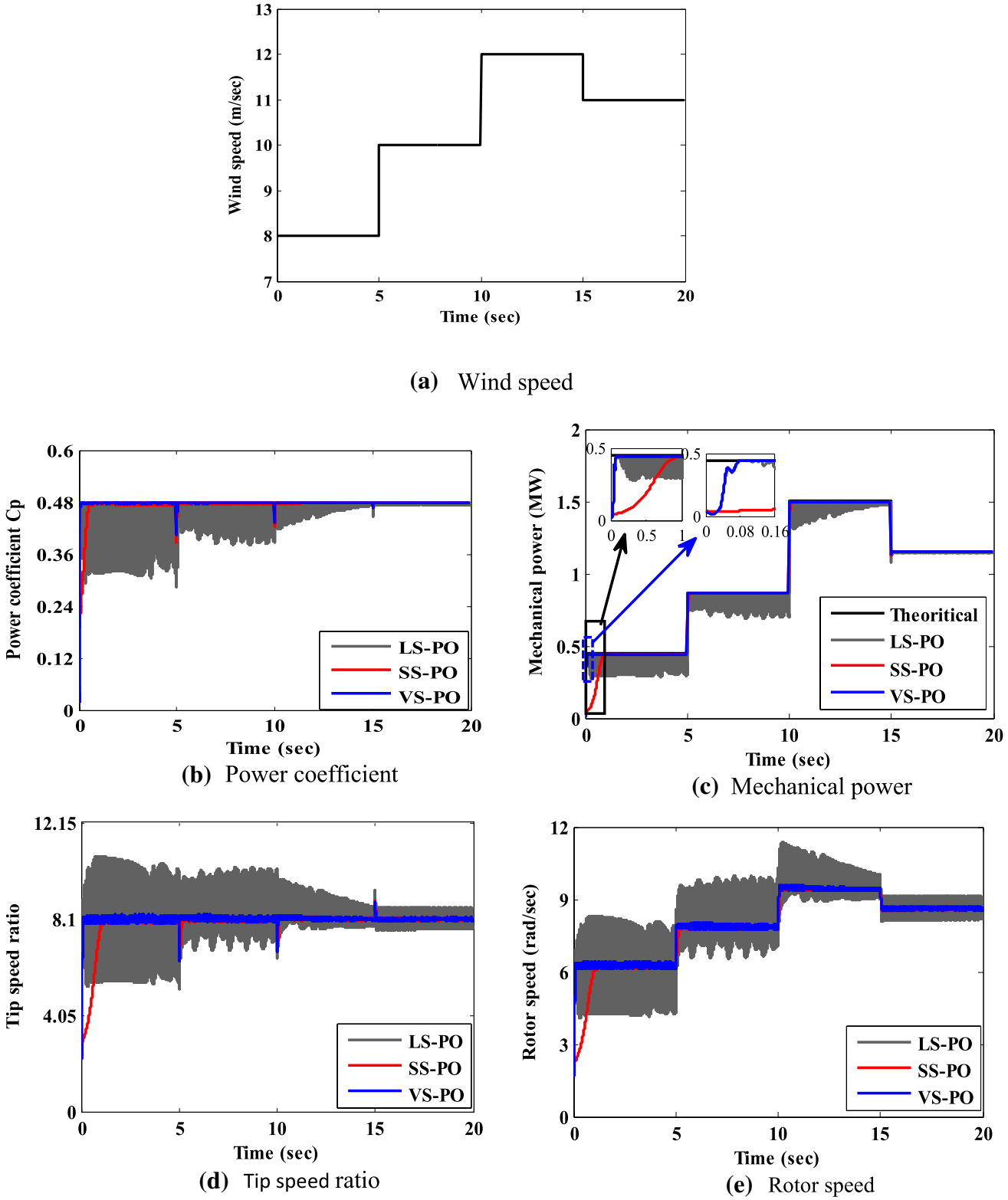

Fig. 7 simulation results under step-change wind speed

LS-PO. Figure 7d shows the optimal tip speed ratio for both conventional and proposed P&O algorithms that are optimally obtained using the VSPO compared to other algorithms. Moreover, the rotor speed follows the optimal rotor speed during wind speed variations as depicted in Fig. 7e. The VSPO shows an effective speed tracking response, and efficiency is increased from 87 to 90.5%. The brief simulation results of all algorithms are listed in Table 2.

8.2 Random wind speed

To test the effectiveness and performance of the proposed VSPO under rapidly changing wind speed, a random wind speed variation is applied as presented in Fig. 8a. The studied profile has average speed and turbulence intensity ratio of (10 m/s) and 20%, respectively. As shown in Fig. 8b, the power coefficient is fairly kept at its optimal value of 0.48 with minimal fluctuation. Hence, the algorithm is able to obtain the MPP. Generally, the SS-PO experiences slow response to the wind speed, while the LS-PO

Table 2 Performance of the conventional and proposed P&O MPPT algorithm

MPPT algorithm	Speed ripple (P. P) (rad/s)	$\Delta\omega$ (rad/s)	Settling time (m/s)	η_{sys} (%)
Conventional small fixed-step P&O	0.02	$\Delta\omega_1 = 0.01$	1200	87
Conventional Large fixed-step P&O	4	$\Delta\omega_1 = 0.2$	80	–
Four-sector P&O [34]	0.02	$\Delta\omega_1 = 0.01$ $\Delta\omega_2 = 0.1$	300	90
Proposed technique	0.02	Shown in Table 2	80	90.5

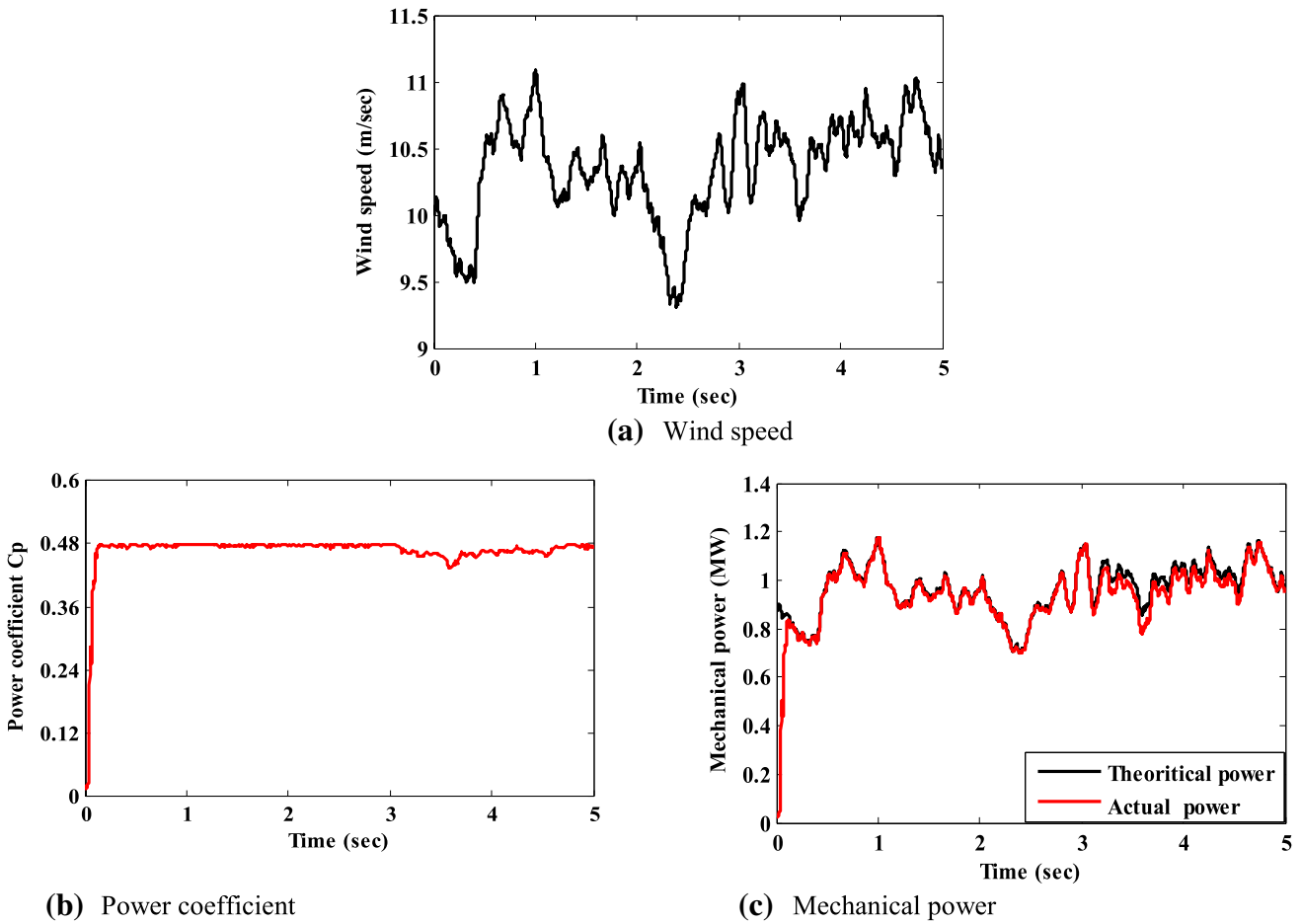

Fig. 8 simulation results under random wind speed

is characterized by a fast response; however, the system suffers large oscillations level [46]. As compared to the CPO techniques, the proposed algorithm shows fast response with small steady-state oscillation. Figure 8c illustrates the performance of the proposed algorithm in extracting the maximum mechanical power.

8.3 Real wind speed

To cope with wind speed nature and investigate the proposed VSPO performance, a one day of real wind speed data is used at a one-hour interval over one day as depicts in Fig. 9a. The real wind speed profile for 24 h is attained from Hokkaido Island, Japan. Below rated wind speed, the proposed VSPO MPPT maintains the optimal value of the power coefficient and tip speed ratio as shown in Fig. 9b, c, respectively. Moreover, they are reduced to minimize the mechanical stress on the WT blades and safety necessity above rated wind speed, while the mechanical power tracks the reference below rated wind speed and is limited to the rated power above rated wind speed as shown in Fig. 9d. The proposed algorithm is considered a vital solution to handle the drawbacks of conventional P&O algorithms and to enhance operation of modified P&O algorithms.

9 Conclusion

Motivated by the limitations of conventional fixed-step-size P&O techniques, this paper proposed a variable-step-size modular sector P&O algorithm. The developed algorithm splits the *P*–*ω* characteristic curve of WT into modular sectors and determines the perturbation step size by comparing a suggested ratio, which depends on the optimal rotor speed with a specified ratio which is specified according to the required power accuracy. The algorithm monitors the position of the operating sector with

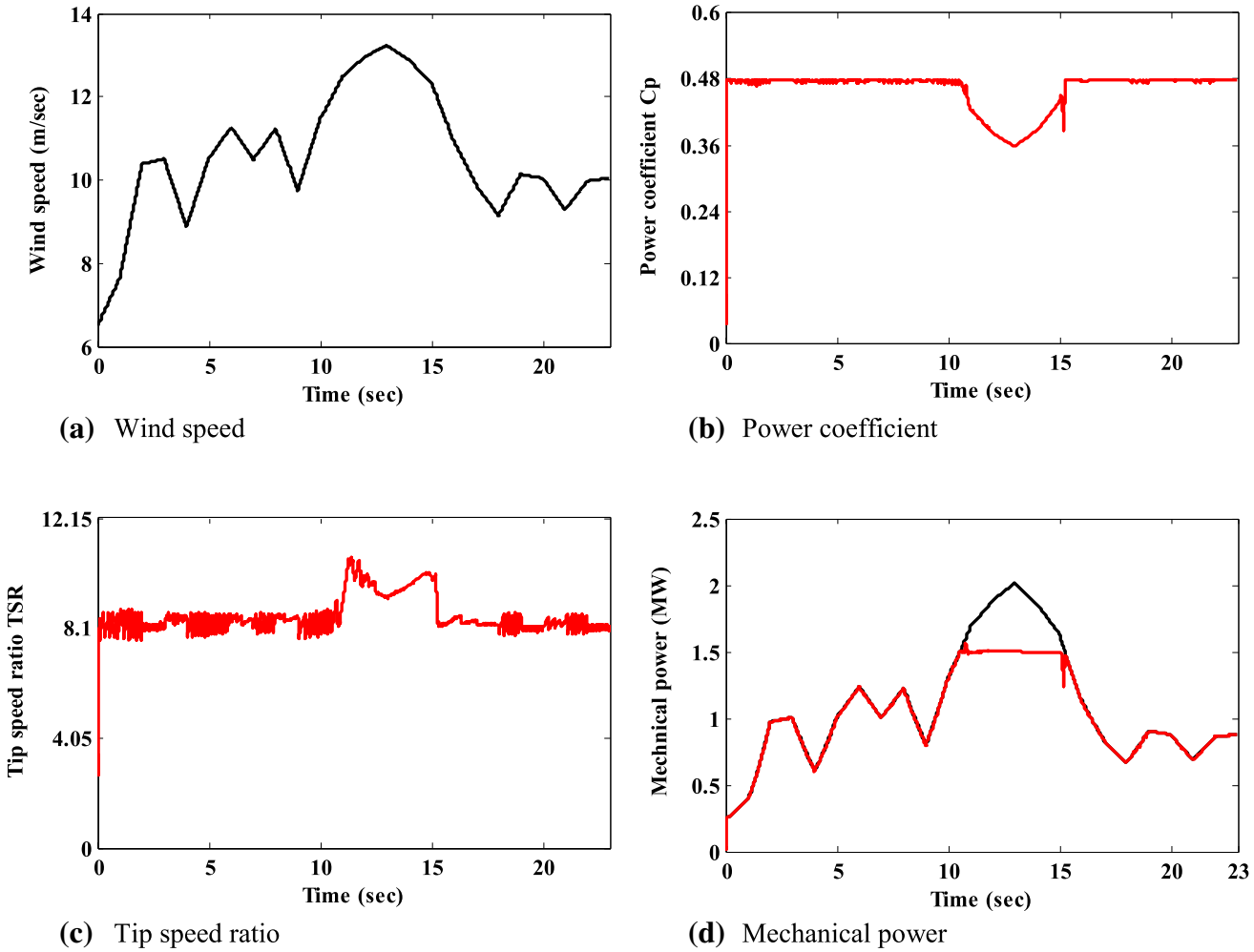

Fig. 9 Simulation results under real wind speed

the MPP sector. A large step size is applied for sectors far away from the MPP to the settling time, while a small step size is employed when approaching the MPP to mitigate the power oscillation. The developed algorithm is tested under various wind speed profiles, and its superior performance compared to the conventional P&O techniques is verified. The VSPO algorithms offer faster tracking speed with lower steady-state oscillation around the MPP, resulting in enhancement of the overall system efficiency. The system efficiency is improved from 87 (with conventional P&O) to 90.5%. The algorithm is tested on a developed MATLAB/SIMULINK model of a 1.5 MW WECS based on three-phase PMSG.

Compliance with ethical standards

Conflict of interest The authors declare that they have no conflict of interest.

Appendix 1

See Table 3.

Table 3 System parameters

Specification of wind turbine		
The coefficients C1 to C6	$C_1 = 0.5176$	$C_2 = 116$
	$C_3 = 0.4$	$C_4 = 5$
	$C_5 = 21$	$C_6 = 0.0068$
Blade radius	$R = 35.25$ m	
Air density	$\rho = 1.225$ kg/m^3	
Optimal tip speed ratio	$\lambda_{opti} = 8.1$	
Maximum power Coefficient	C_{p-}max $= 0.48$	
PMSG parameters		
Rated power	$P = 1.5$ MW	
Pole pairs number	$n_p = 40$	
Stator resistance	$R_s = 3.17$ mΩ	
Stator inductance	$L_s = 3.07$ mH	
Moment of inertia	$J = 10000$ kg m^2	
Flux linkage	$\psi = 7.0172$ wb	
DC bus and gird parameters		
Dc link voltage	$V_{dc} = 1150$ V	
Capacitor of the DC link	$C = 0.023$ F	
Grid voltage	$V_g = 575$ V	
Grid frequency	$F = 60$ Hz	
Grid resistance	$R_g = 0.003$ pu	
Grid inductance	$L_g = 0.3$ pu	

Appendix 2

See Table 4.

Table 4 PI-controller parameters

MSC PI Controller		
K_p	50	
K_i	10	
GSC PI- controller		
DC link control	K_{p_Vdc}	8
	K_{i_Vdc}	400
D-axis current control	K_{p_id}	0.83
	K_{i_id}	5
Q-axis current control	K_{p_iq}	0.83
	K_{i_iq}	5

References

1. Akbari M-A, Aghaei J, Barani M (2017) Convex probabilistic allocation of wind generation in smart distribution networks. IET Renew Power Gener 11:1211–1218
2. Waqas H, Khan SU, Imran M, Bhatti M (2019) Thermally developed Falkner-Skan bioconvection flow of a magnetized nanofluid in the presence of a motile gyrotactic microorganism: buongiorno's nanofluid model. Phys Scr 94:115304
3. Marin M, Vlase S, Ellahi R, Bhatti M (2019) On the partition of energies for the backward in time problem of thermoelastic materials with a dipolar structure. Symmetry 11:863
4. Mendecka B, Lombardi L, Stanek W (2018) Analysis of life cycle thermo-ecological cost of electricity from wind and its application for future incentive mechanism. Energy Convers Manag 170:73–81
5. Hossain MM, Ali MH (2015) Future research directions for the wind turbine generator system. Renew Sustain Energy Rev 49:481–489
6. Xie D, Lu Y, Sun J, Gu C (2017) Small signal stability analysis for different types of PMSGs connected to the grid. Renew Energy 106:149–164
7. Kumar D, Chatterjee K (2016) A review of conventional and advanced MPPT algorithms for wind energy systems. Renew Sustain Energy Rev 55:957–970
8. Yang B, Yu T, Shu H, Zhang Y, Chen J, Sang Y, Jiang L (2018) Passivity-based sliding-mode control design for optimal power extraction of a PMSG based variable speed wind turbine. Renew Energy 119:577–589
9. Justo JJ, Mwasilu F, Jung J-W (2015) Doubly-fed induction generator based wind turbines: a comprehensive review of fault ride-through strategies. Renew Sustain Energy Rev 45:447–467
10. Saeed MS, Mohamed EE (2017) Partitioned stator doubly-fed brushless reluctance machine for wind generating systems. In: Power systems conference (MEPCON), 2017 Nineteenth International Middle East, pp 864–869
11. Tripathi S, Tiwari A, Singh D (2015) Grid-integrated permanent magnet synchronous generator based wind energy conversion systems: a technology review. Renew Sustain Energy Rev 51:1288–1305

12. Yaramasu V, Dekka A, Durán MJ, Kouro S, Wu B (2017) PMSG-based wind energy conversion systems: survey on power converters and controls. IET Electr Power Appl 11:956–968
13. Yaramasu V, Wu B (2014) Predictive control of a three-level boost converter and an NPC inverter for high-power PMSG-based medium voltage wind energy conversion systems. IEEE Trans Power Electron 29:5308–5322
14. Vazquez S, Leon JI, Franquelo LG, Rodriguez J, Young HA, Marquez A, Zanchetta P (2014) Model predictive control: a review of its applications in power electronics. IEEE Ind Electron Mag 8:16–31
15. Yaramasu V, Wu B, Rivera M, Rodriguez J (2014) A new power conversion system for megawatt PMSG wind turbines using four-level converters and a simple control scheme based on two-step model predictive strategy—Part II: simulation and experimental analysis. IEEE J Emerg Sel Top Power Electron 2:14–25
16. Yaramasu V, Wu B, Alepuz S, Kouro S (2014) Predictive control for low-voltage ride-through enhancement of three-level-boost and NPC-converter-based PMSG wind turbine. IEEE Trans Ind Electron 61:6832–6843
17. Gebraad P, Van Wingerden J (2015) Maximum power-point tracking control for wind farms. Wind Energy 18:429–447
18. Castelló J, Espí JM, García-Gil R (2016) Development details and performance assessment of a wind turbine emulator. Renew Energy 86:848–857
19. Ganjefar S, Ghassemi AA, Ahmadi MM (2014) Improving efficiency of two-type maximum power point tracking methods of tip-speed ratio and optimum torque in wind turbine system using a quantum neural network. Energy 67:444–453
20. Lalouni S, Rekioua D, Idjdarene K, Tounzi A (2014) An improved MPPT algorithm for wind energy conversion system. J Electr Syst 10:484–494
21. Zhao Y, Wei C, Zhang Z, Qiao W (2013) A review on position/speed sensorless control for permanent-magnet synchronous machine-based wind energy conversion systems. IEEE J Emerg Sel Top Power Electron 1:203–216
22. Urtasun A, Sanchis P, Marroyo L (2014) Small wind turbine sensorless MPPT: robustness analysis and lossless approach. IEEE Trans Ind Appl 50:4113–4121
23. Abdullah MA, Yatim A, Tan CW, Saidur R (2012) A review of maximum power point tracking algorithms for wind energy systems. Renew Sustain Energy Rev 16:3220–3227
24. Lahfaoui B, Zouggar S, Elhafyani ML, Seddik M (2015) Experimental study of P&O MPPT control for wind PMSG turbine. In: 2015 3rd International renewable and sustainable energy conference (IRSEC), pp 1–6
25. Lahfaoui B, Zouggar S, Mohammed B, Elhafyani ML (2017) Real time study of P&O MPPT control for small wind PMSG turbine systems using arduino microcontroller. Energy Procedia 111:1000–1009
26. Yu KN, Liao CK (2015) Applying novel fractional order incremental conductance algorithm to design and study the maximum power tracking of small wind power systems. J Appl Res Technol 13:238–244
27. Kanathipan K, Lam J (2017) A new modified maximum power extraction technique for wind and hybrid renewable energy systems. In: Electrical power and energy conference (EPEC), 2017 IEEE, pp 1–6
28. Daili Y, Gaubert J-P, Rahmani L (2015) Implementation of a new maximum power point tracking control strategy for small wind energy conversion systems without mechanical sensors. Energy Convers Manag 97:298–306
29. Kazmi SMR, Goto H, Guo H-J, Ichinokura O (2011) A novel algorithm for fast and efficient speed-sensorless maximum power point tracking in wind energy conversion systems. IEEE Trans Ind Electron 58:29–36
30. Agarwal V, Aggarwal RK, Patidar P, Patki C (2010) A novel scheme for rapid tracking of maximum power point in wind energy generation systems. IEEE Trans Energy Convers 25:228–236
31. Harrag A, Messalti S (2015) Variable step size modified P&O MPPT algorithm using GA-based hybrid offline/online PID controller. Renew Sustain Energy Rev 49:1247–1260
32. Chen J, Lin T, Wen C, Song Y (2016) Design of a unified power controller for variable-speed fixed-pitch wind energy conversion system. IEEE Trans Ind Electron 63:4899–4908
33. Linus RM, Damodharan P (2015) Maximum power point tracking method using a modified perturb and observe algorithm for grid connected wind energy conversion systems. IET Renew Power Gener 9:682–689
34. Putri RI, Pujiantara M, Priyadi A, Ise T, Purnomo MH (2017) Maximum power extraction improvement using sensorless controller based on adaptive perturb and observe algorithm for PMSG wind turbine application. IET Electr Power Appl 12:455–462
35. Wang P, Liu F, Song Y (2013) A novel maximum power point tracking control method in wind turbine application. In: Control Conference (CCC), 2013 32nd Chinese, pp 7569–7574
36. Kortabarria I, Andreu J, de Alegría IM, Jiménez J, Gárate JI, Robles E (2014) A novel adaptative maximum power point tracking algorithm for small wind turbines. Renew Energy 63:785–796
37. Mousa HH, Youssef A-R, Mohamed EE (2019) Variable step size P&O MPPT algorithm for optimal power extraction of multi-phase PMSG based wind generation system. Int J Electr Power Energy Syst 108:218–231
38. Karabacak M (2019) A new perturb and observe based higher order sliding mode MPPT control of wind turbines eliminating the rotor inertial effect. Renew Energy 133:807–827
39. Mousa HH, Youssef A-R, Mohamed EE (2019) Adaptive P&O MPPT algorithm based wind generation system using realistic wind fluctuations. Int J Electr Power Energy Syst 112:294–308
40. Uddin MN, Amin IK (2019) Adaptive step size based hill-climb search algorithm for MPPT control of DFIG-WECS with reduced power fluctuation and improved tracking performance. Electr Power Compon Syst 46:1–15
41. Mousa H, Youssef A-R, Mohamed E (2019) Study of robust adaptive step-sizes P&O MPPT algorithm for high inertia WT with direct driven multi-phase PMSG. Int Trans Electr Energy Syst 29(10):e12090
42. Chen J, Yao W, Zhang C-K, Ren Y, Jiang L (2019) Design of robust MPPT controller for grid-connected PMSG-Based wind turbine via perturbation observation based nonlinear adaptive control. Renew Energy 134:478–495
43. Mousa HH, Youssef A-R, Mohamed EE (2020) Hybrid and adaptive sectors P&O MPPT algorithm based wind generation system. Renew Energy 145:1412–1429
44. Shotorbani AM, Mohammadi-Ivatloo B, Wang L, Marzband M, Sabahi M (2019) Application of finite-time control Lyapunov function in low-power PMSG wind energy conversion systems for sensorless MPPT. Int J Electr Power Energy Syst 106:169–182
45. Yang B, Yu T, Shu H, Zhang X, Qu K, Jiang L (2018) Democratic joint operations algorithm for optimal power extraction of PMSG based wind energy conversion system. Energy Convers Manag 159:312–326
46. Youssef A-R, Ali AI, Saeed MS, Mohamed EE (2019) Advanced multi-sector P&O maximum power point tracking technique for wind energy conversion system. Int J Electr Power Energy Syst 107:89–97
47. Mousa H, Youssef A-R, Mohamed E (2019) Optimal power extraction control schemes for five-phase PMSG based

wind generation systems. Eng Sci Technol Int J. https://doi.org/10.1016/j.jestch.2019.04.004
48. Dahbi A, Nait-Said N, Nait-Said M-S (2016) A novel combined MPPT-pitch angle control for wide range variable speed wind turbine based on neural network. Int J Hydrogen Energy 41:9427–9442
49. Rolan A, Luna A, Vazquez G, Aguilar D, Azevedo G (2009) Modeling of a variable speed wind turbine with a permanent magnet synchronous generator. In: IEEE international symposium on industrial electronics, 2009. ISIE 2009, pp 734–739
50. Rodriguez J, Kazmierkowski MP, Espinoza JR, Zanchetta P, Abu-Rub H, Young HA, Rojas CA (2013) State of the art of finite control set model predictive control in power electronics. IEEE Trans Ind Inf 9:1003–1016
51. Jena D, Rajendran S (2015) A review of estimation of effective wind speed based control of wind turbines. Renew Sustain Energy Rev 43:1046–1062
52. Mousa HH, Youssef AR, Mohamed EE (2019) Model predictive speed control of five-phase permanent magnet synchronous generator-based wind generation system via wind-speed estimation. Int Trans Electr Energy Syst 29:e2826
53. Ali AI, Sayed MA, Mohamed EE (2018) Modified efficient perturb and observe maximum power point tracking technique for grid-tied PV system. Int J Electr Power Energy Syst 99:192–202
54. Shehata E (2017) A comparative study of current control schemes for a direct-driven PMSG wind energy generation system. Electr Power Syst Res 143:197–205